Clinical Cancer Research

Development and Validation of a Combined Hypoxia and Immune Prognostic Classifier for Head and Neck Cancer

Jill M. Brooks[1,2], Albert N. Menezes[2], Maha Ibrahim[2,3], Lucinda Archer[4], Neeraj Lal[5], Christopher J. Bagnall[6], Sandra V. von Zeidler[7], Helen R. Valentine[8], Rachel J. Spruce[1,2], Nikolaos Batis[1,2], Jennifer L. Bryant[1,2], Margaret Hartley[1,2], Baksho Kaul[9], Gordon B. Ryan[1,2], Riyue Bao[10], Arun Khattri[10], Steven P. Lee[5], Kalu U.E. Ogbureke[11], Gary Middleton[5], Daniel A. Tennant[9], Andrew D. Beggs[2], Jonathan Deeks[4,12], Catharine M. L. West[8], Jean-Baptiste Cazier[2], Benjamin E. Willcox[5], Tanguy Y. Seiwert[10], and Hisham Mehanna[1,2]

Abstract

Purpose: Intratumoral hypoxia and immunity have been correlated with patient outcome in various tumor settings. However, these factors are not currently considered for treatment selection in head and neck cancer (HNC) due to lack of validated biomarkers. Here we sought to develop a hypoxia-immune classifier with potential application in patient prognostication and prediction of response to targeted therapy.

Experimental Design: A 54-gene hypoxia-immune signature was constructed on the basis of literature review. Gene expression was analyzed *in silico* using the The Cancer Genome Atlas (TCGA) HNC dataset ($n = 275$) and validated using two independent cohorts ($n = 130$ and 123). IHC was used to investigate the utility of a simplified protein signature. The spatial distribution of hypoxia and immune markers was examined using multiplex immunofluorescence staining.

Results: Unsupervised hierarchical clustering of TCGA dataset (development cohort) identified three patient subgroups with distinct hypoxia-immune phenotypes and survival profiles: hypoxia[low]/immune[high], hypoxia[high]/immune[low], and mixed, with 5-year overall survival (OS) rates of 71%, 51%, and 49%, respectively ($P = 0.0015$). The prognostic relevance of the hypoxia-immune gene signature was replicated in two independent validation cohorts. Only PD-L1 and intratumoral CD3 protein expression were associated with improved OS on multivariate analysis. Hypoxia[low]/immune[high] and hypoxia[high]/immune[low] tumors were over-represented in "inflamed" and "immune-desert" microenvironmental profiles, respectively. Multiplex staining demonstrated an inverse correlation between CA-IX expression and prevalence of intratumoral CD3^{+} T cells ($r = -0.5464$; $P = 0.0377$), further corroborating the transcription-based classification.

Conclusions: We developed and validated a hypoxia-immune prognostic transcriptional classifier, which may have clinical application to guide the use of hypoxia modification and targeted immunotherapies for the treatment of HNC.

Introduction

Head and neck cancer (HNC) is the sixth most common cancer worldwide, with an annual incidence of around 600,000 cases. It has a poor outcome with a 5-year mortality rate of around 50% (1). The main risk factors include smoking, alcohol, and infection with high-risk human papillomaviruses (HPV), the latter conferring considerably better survival outcomes than the former two (2).

While many prognostic biomarkers have been described previously (2, 3), all include a combination of clinical factors and HPV status, and currently there is no widely accepted molecular classification. Importantly, there are no treatment response

[1]Institute of Head and Neck Studies and Education, University of Birmingham, Birmingham, United Kingdom. [2]Institute of Cancer and Genomic Sciences, University of Birmingham, Birmingham, United Kingdom. [3]South Egypt Cancer Institute, Assiut University, Assiut, Egypt. [4]Institute of Applied Health Research, University of Birmingham, Birmingham, United Kingdom. [5]Institute of Immunology and Immunotherapy, University of Birmingham, Birmingham, United Kingdom. [6]Human Biomaterials Resource Centre, University of Birmingham, Birmingham, United Kingdom. [7]Department of Pathology, Federal University of Espírito Santo, Espírito Santo, Brazil. [8]Division of Cancer Sciences, University of Manchester, Christie Hospital, Manchester Academic Health Science Centre, Manchester, United Kingdom. [9]Institute of Metabolism and Systems Research, University of Birmingham, Birmingham, United Kingdom. [10]The University of Chicago Medicine, Chicago, Illinois. [11]Department of Diagnostic and Biomedical Sciences, The University of Texas Health Science Center at Houston, Houston, Texas. [12]NIHR Birmingham Biomedical Research Centre, University of Birmingham and University Hospitals Birmingham NHS Foundation Trust, Birmingham, United Kingdom.

AACR 5315

Brooks et al.

Translational Relevance

Comprehensive genomic characterization of head and neck cancer (HNC) has identified subgroups of tumors with distinct molecular and biological properties. Current standard-of-care treatment for HNC does not consider these fundamental differences. This largely reflects the absence of validated biomarkers for selection of standard and/or new targeted therapies based on individual tumor biology. Focusing on two biological properties: hypoxia status and immune profile, we developed and validated a prognostic transcriptional classifier, which stratifies patients with HNC into three distinct hypoxia-immune phenotypes and survival profiles: hypoxia^{high}/immune^{low}, hypoxia^{low}/immune^{high}, and a mixed group. Multiplex immunofluorescence staining demonstrated an inverse spatial distribution of hypoxia- and immune-response markers, corroborating our subtype classification based on gene expression. Each of the three subtypes has distinct molecular, histologic, and biologic characteristics, likely to be driven by distinct targetable pathways, for which potentially effective therapies (e.g., hypoxia modification, EGFR inhibition, and immune checkpoint blockade) have been demonstrated in HNC.

classifiers. As a result, patients receive treatment based on disease stage and patient/clinician preference, rather than on the biology of the tumor.

Recently, there have been advances in our understanding of the biologic and molecular characteristics of HNC. A comprehensive multi-platform genomic characterization by The Cancer Genome Atlas (TCGA) Network confirmed four previously defined subtypes: classical, mesenchymal, basal, and atypical (4–6). A more recent study identified five subgroups: HPV-positive mesenchymal, non-HPV mesenchymal, HPV classical, non-HPV classical, and basal (non-HPV) subtypes (7). When combined, the findings of these studies suggest three main subgroups: an inflamed/mesenchymal subtype demonstrates high expression of immune response genes and mesenchymal markers. A classical subtype (regardless of HPV status) has increased genomic aberrations associated with tobacco use. Finally, a basal subtype is highly enriched for hypoxia signaling with a lack of immune-related markers. Hypoxia is known to induce immunosuppression, both directly (e.g., via inhibition of T-cell proliferation and effector cytokine production) and indirectly (e.g., through metabolic competition, upregulation of coinhibitory receptors, or recruitment/conversion of immunosuppressive cell populations; refs. 8–14). Furthermore, HIF-1α signaling can be switched on by EGFR signaling (15, 16), which was also increased in some basal cancers.

Using this as a basis for a molecular classification, we then researched the availability of potential therapeutic paradigms for each of the subgroups. Hypoxic modifiers have been shown to have significant effects on survival in HNC (17, 18). More recently, evidence has emerged for the efficacy of immune checkpoint inhibitors in HNC (19, 20).

Combining these together, we sought to develop and validate a prognostic molecular classifier, based on immune response and hypoxia status, first *in silico* from fresh-frozen tissues, and then using targeted RNA sequencing of formalin-fixed, paraffin-

embedded (FFPE) tissue samples to facilitate ease of clinical application. We then evaluated whether an IHC-based signature could substitute for, and simplify, the developed molecular signature, to further facilitate clinical implementation and cost reduction.

Materials and Methods

Patient cohorts and samples

The *in silico* discovery cohort (characteristics and treatment detailed in Table 1 and Supplementary Table S1, respectively: TCGA) comprised samples from the HNC dataset in the TCGA, which contains whole-transcriptome gene expression data from fresh-frozen samples. Because HPV positivity is an independent prognostic factor for HNC (2), only cases with known HPV status

Table 1. Baseline characteristics of patients in the discovery and validation cohorts

	TCGA cohort n = 275 Number (%)	Chicago cohort n = 134 Number (%)[a]	Correlate cohort n = 163 Number (%)
Age at diagnosis (y)			
median (range)	62 (19–90)	57 (33–81)	57 (35–84)
Gender			
Male	199 (72.4)	107 (82.3)	116 (71.2)
Female	76 (27.6)	23 (17.7)	46 (28.2)
Not known	0 (0.0)	0 (0.0)	1 (0.6)
Tobacco use			
Never	51 (18.6)	19 (14.6)	36 (22.1)
Light	34 (12.4)	35 (26.9)	29 (17.8)
Heavy	183 (66.5)	73 (56.2)	85 (52.1)
Not known	7 (2.5)	3 (2.3)	13 (8.0)
Alcohol consumption			
Never	85 (30.9)	15 (11.5)	19 (11.7)
Light	184 (66.9)	54 (41.5)	85 (52.1)
Heavy		60 (46.2)	37 (22.7)
Not known	6 (2.2)	1 (0.8)	22 (13.5)
Anatomic site			
Oral cavity	169 (61.5)	25 (19.2)	1 (0.6)
Oropharynx	32 (11.6)	73 (56.1)	162 (99.4)
Hypopharynx	2 (0.7)	8 (6.2)	0 (0.0)
Larynx	71 (25.8)	24 (18.5)	0 (0.0)
Other	1 (0.4)	0 (0.0)	0 (0.0)
T-stage (TNM7)			
T1	13 (4.7)	8 (6.2)	33 (20.2)
T2	84 (30.6)	37 (28.4)	59 (36.2)
T3	82 (29.8)	29 (22.3)	35 (21.5)
T4	96 (34.9)	55 (42.3)	28 (17.2)
Not known	0 (0.0)	1 (0.8)	8 (4.9)
N-stage (TNM7)			
N0	136 (49.4)	12 (9.2)	17 (10.4)
N1	49 (17.8)	10 (7.7)	17 (10.4)
N2	81 (29.5)	92 (70.7)	107 (65.6)
N3	6 (2.2)	14 (10.8)	11 (6.8)
N4	0 (0.0)	1 (0.8)	0 (0.0)
Not known	3 (1.1)	1 (0.8)	11 (6.8)
Clinical stage			
I	9 (3.3)	2 (1.5)	7 (4.3)
II	57 (20.7)	0 (0.0)	5 (3.1)
III	65 (23.6)	3 (2.3)	17 (10.4)
IV	144 (52.4)	124 (95.4)	125 (76.7)
Not known	0 (0.0)	1 (0.8)	9 (5.5)
HPV status[b]			
Positive	36 (13.1)	57 (42.5)	93 (57.1)
Negative	239 (86.9)	77 (57.5)	70 (42.9)

[a]Clinical data not available for four cases.
[b]HPV status for correlate, based on p16 expression.

were considered; this yielded a cohort of 275 patients, the majority being HPV negative.

The *in silico* validation cohort comprised microarray gene expression data for fresh-frozen samples from 134 patients with locoregionally advanced HNC [ref. 7; detailed in Table 1; Supplementary Table S1 (Chicago)], including both HPV-positive and -negative cases.

We then evaluated FFPE diagnostic biopsy or surgical resection samples from a retrospective cohort of 163 patients with oropharyngeal cancer, recruited to the PET-NECK or Predictr clinical studies (Table 1; Supplementary Table S1, Correlate). A cohort of 12 patients who underwent tonsillectomy for management of a nonmalignant process (snoring), recruited via the Oromouth study, served as controls. Ethical approval for use of tissue samples in translational research was granted by North West - Preston Research Ethics Committee (Reference: 16/NW/0265). p16 expression was utilized as a surrogate marker for HPV status. IHC staining for p16 was performed using the CINtec Histology Kit (Roche Laboratories); samples with ≥70% strong diffuse nuclear and cytoplasmic staining of tumor cells were considered positive (21).

Studies were conducted in accordance with the Declaration of Helsinki. Patients gave informed written consent to participate or anonymized samples were used in accordance with Human Tissue Act rules of the United Kingdom, and the above Research Ethics Committee approval.

In silico development and validation of an RNA signature

For *in silico* development, expression data for genes comprising the hypoxia (Eustace and colleagues; ref. 22) and immune signatures (CIRC; ref. 23), plus additional genes of interest (including other immune-related genes and genes frequently mutated in HNC; Supplementary Table S2) were filtered from HT-seq gene count files downloaded from the TCGA HNC dataset (ref. 6, https://portal.gdc.cancer.gov/projects/TCGA-HNSC). Each dataset was normalized by dividing the expression values by the sum of expression values of the analyzed genes for each sample, then $\log_2$ transformed; z-scores were calculated for these values using R v3.3.2 (https://www.r-project.org/).

Cluster analyses for genes/samples were obtained from the $\log_2$ values matrix for each dataset using Spearman distance and Ward criterion in R. These clusters were then used to plot heatmaps using the z-score values matrix for color intensities. Survival was assessed by Cox regression analyses using Kaplan–Meier curves to compare the three highest hierarchical sample groups on each heatmap. In addition, a Cox regression multivariate was used to calculate the combined effect of HPV status and heatmap groups, using the Survival package in R (https://cran.r-project.org/web/packages/survival/index.html). Outcome measure was overall survival (OS) from treatment end date to death or last follow-up and censure.

For *in silico* validation, data from a previously published cohort (7) were interrogated for expression of the above gene signatures. Data for four genes *COL4A6* (Eustace and colleagues), *CD80*, *IFNG*, and *PDCD1LG2* (CIRC) were unavailable.

Sample size calculation

Using the data from the development TCGA cohort, to identify a difference of 25% in 3-year survival (from 75% immune[high] to 50% hypoxia[high] and mixed groups) with a power of 80% and a two-sided alpha of 0.05, we would require 138 cases; at 85% or 90% power we would require 158 or 185 cases, respectively (using the Kelsey calculation method and OpenEpi v3.0 software).

External validation of RNA signature using FFPE samples

Targeted RNA sequencing. Gene expression was quantified using Illumina TruSeq Targeted RNA technology. RNA was extracted from 3–8 FFPE sections of 10 μm thickness using the PureLink FFPE RNA Isolation Kit (Thermo Fisher Scientific), DNase treated, and then quantified using the Qubit RNA BR Assay Kit (Thermo Fisher Scientific). Libraries were prepared using a TruSeq Targeted RNA Custom Panel Kit (Illumina), according to the manufacturer's instructions. The panel comprised 83 genes (see Supplementary Table S2 for full details). The resultant libraries were pooled and sequenced using the Illumina MiSeq platform, with a MiSeq reagent kit v3 150 cycle and paired end reads.

Data analysis. Quality assessment and filtering of the reads were carried out using FastQC v0.11.2 (http://www.bioinformatics.babraham.ac.uk/projects/fastqc) and PrinSeq Lite v0.20.4 (http://prinseq.sourceforge.net/), respectively. Reads were aligned to appropriate reference gene sequences obtained from GenBank (see Supplementary Table S2 for reference numbers), using BWA samse v0.7.15 (http://bio-bwa.sourceforge.net/). The obtained SAM files were then sorted and indexed using SAMtools v1.2 (http://samtools.sourceforge.net/) and read count by gene files was obtained using subread featureCounts v1.5.0-p1 (http://subread.sourceforge.net/). The expression matrix comprising genes within the analyzed signatures was then submitted to a similar normalization and analysis as described for the discovery dataset.

Histology and IHC

All staining was performed on FFPE sections of 4- to 5-μm thickness. Hematoxylin and eosin (H & E) staining was carried out using a Leica Autostainer xl on program 1. Automated IHC staining was carried out using a Leica Bond Max with standard F protocol and the following primary antibodies: Novocastra Liquid Mouse Monoclonal CA-IX Antibody clone TH22 (Leica Biosystems), 1:100 dilution; PD-L1 (E1L3N) XP Rabbit mAb (Cell Signaling Technology), 1:200 dilution.

For manual IHC staining, sections were deparaffinized in xylene then rehydrated in graded concentrations of alcohol. Following heat-induced epitope retrieval, slides were stained using the Novolink Polymer Detection System (Leica Biosystems) and the following primary antibodies: FLEX ready-to-use polyclonal rabbit anti-human CD3 (Dako) and mouse monoclonal anti-human LAG3 Antibody clone 17B4 (LSBio), 1:250 dilution.

IHC scoring. IHC slides were scored independently by two trained calibrated pathologists; when scoring was discrepant, slides were rescored and a consensus reached. H & E slides were scored for tumor-infiltrating lymphocytes (TIL) as described by Ward and colleagues (3). CD3 was semiquantitatively estimated (range 1–4) using the mean score from three representative high power fields, where 1 = no, or sporadic CD3$^+$ cells, 2 = moderate numbers of CD3$^+$ cells, 3 = abundant occurrence of CD3$^+$ cells, and 4 = highly abundant occurrence of CD3$^+$ cells; and was evaluated separately for three regions: intratumoral, peritumoral stroma, and tumor advancing margin (adapted from ref. 24). Median values were used for survival analysis dichotomization.

Cases were also assigned an immune profile (desert, excluded, or inflamed; ref. 25) based on CD3 expression using the following cutoffs: immune desert, score of <2 in all regions; immune excluded, difference of >1 between stromal versus intratumoral score; immune inflamed, score of ≥ 2 in two or more regions.

PD-L1 was evaluated on both tumor cells and immune-infiltrating cells (morphologically identified as lymphocytes and macrophages/dendritic cells; adapted from refs. 26, 27). For tumor cells, the percentage of positive cells was estimated for whole sections; four different cutoffs defining positivity were considered: $\geq 1\%$, $\geq 5\%$, $\geq 25\%$, and $\geq 50\%$ (28). The pattern of staining was also recorded, as either constitutive (most/all of tumor cells positive) or inductive (peripheral staining on the interface between tumor and stroma or discrete regions of staining within tumor nests). Immune cells within tumor nests or within the peritumoral stroma were semiquantitatively scored as follows: 0 = negative, 1 = low abundance, and 2 = high abundance. Tumor and inflammatory cell expression were also pooled to give a combined positive score (CPS). The presence/absence of immune cells surrounding the tumor and forming a PD-L1–positive cordon was also noted.

LAG3 expression on tumor-infiltrating immune cells was scored as the mean percentage of positive cells from 10 high power fields for two regions: intratumoral and peritumoral. CA-IX was evaluated for tumor cells only; the percentage of positive cells was estimated on whole sections. For both LAG3 and CA-IX, four different cutoffs defining positivity were considered: $\geq 1\%$, $\geq 5\%$, $\geq 25\%$, and $\geq 50\%$.

IHC data analysis. Univariable Cox regression was used to identify IHC factors associated with OS. Follow-up was censored at 60 months in all analyses. Variables were analyzed as linear continuous measures and dichotomized according to prestated thresholds. Survival by category for each marker is displayed in Kaplan–Meier plots. Multivariable Cox regression models assessed whether prognostic value was altered with adjustments for important clinical factors (age, gender, T stage, N stage, p16 status, smoking status, and alcohol consumption). Analysis was conducted as complete case (123/161 patients), and using multiple imputation with chained equations (24 imputations) to impute missing data. All analyses were performed using Stata 15.

Multiplex staining. Multi-color immunofluorescent staining was carried out on the Leica Bond Rx using an Opal 7-color fIHC kit and the following primary antibody fluorochrome combinations: CD3/Opal 520, CA-IX/Opal 570, PD-L1/Opal 650, and CK [monoclonal mouse anti-human cytokeratin (concentrate) antibody clone AE1/AE3]/Opal 650. Staining was imaged with the Vectra Automated Quantitative Pathology Imaging System, and 7–11 representative fields per case were quantitatively analyzed using Inform Advanced Image Analysis Software v 2.3 (PerkinElmer).

Results

Development of prognostic classifier

TCGA data from 275 HNC cases (detailed in Table 1; Supplementary Table S1) were interrogated for expression of hypoxia- and immune response–related genes using a combination of two previously developed signatures: a hypoxia signature composed of 26 genes (Eustace and colleagues; ref. 22) and an immune response signature containing 28 genes (CIRC; ref. 23); individual genes are detailed in Supplementary Table S2. Bioinformatics analysis, using unsupervised two-dimensional hierarchical clustering, identified distinct HNC patient subgroups with coordinate expression of hypoxia- and immune response–related genes (Fig. 1A). Three subgroups were classified as follows: (i) hypoxia^high/immune^low, comprised almost exclusively of HPV-negative cases, (ii) hypoxia^low/immune^high, enriched for HPV-positive cases, and (iii) a mixed subgroup, containing both HPV-positive and -negative cases (Fig. 1A; gene ID is provided in Supplementary Fig. S1). Kaplan–Meier analysis revealed that the three subgroups have different survival profiles, with the hypoxia^low/immune^high subgroup having the best prognosis, corresponding to a 5-year OS of 71.4% (Fig. 1B). The hypoxia^high/immune^low and mixed subgroups have similar profiles, with 5-year OS figures of 50.8% and 48.6%, respectively ($P = 0.0015$, HPV-adjusted $P = 0.0005$; adjustment for other standard prognostic variables is considered in Supplementary Table S3). Of note, the hypoxia and immune gene signatures were not independently prognostic (Supplementary Fig. S2). Furthermore, consideration of HPV-negative cases alone, within the predefined hypoxia-immune subgroups, maintained comparable survival profiles ($P = 0.001$).

Validation of prognostic classifier

We then sought to validate the hypoxia-immune signature, first *in silico* using data for 134 HNC cases comprising the previously published Chicago cohort (ref. 7; detailed in Table 1; Supplementary Table S1). Bioinformatics analysis identified comparable patient subgroups with those described above (hypoxia^high/immune^low, hypoxia^low/immune^high, and mixed; Fig. 1C). As described previously, the hypoxia^high/immune^low subgroup was predominantly HPV negative. Although HPV-positive cases were again overrepresented in the hypoxia^low/immune^high subgroup, approximately one third of cases in this group were HPV negative. Likewise, the mixed class comprised both HPV-positive and -negative cases, suggesting that the hypoxia-immune signature classifies beyond HPV status. Correlation of gene expression profiles with survival confirmed that subgroups have distinct outcomes. Here again, the hypoxia^low/immune^high subgroup have the best prognosis, 5-year OS 76.2%, whereas the hypoxia^high/immune^low and mixed classes have inferior outcomes with 5-year OS of 65.1% and 60.0%, respectively, ($P = 0.012$; HPV-adjusted $P = 0.0025$).

The second validation cohort comprised 163 cases of oropharyngeal squamous cell carcinoma; consistent with their anatomic location a higher percentage of cases were HPV positive (Table 1; Supplementary Table S1: Correlate; flow of patient samples through study is summarized in Supplementary Fig. S3). FFPE tissue samples were available from this cohort enabling comparative gene and protein expression analysis. Gene expression was quantified using Illumina TruSeq Targeted RNA technology. Quality control measures, based on a minimum number of mapped reads of 70,000, reduced the number of informative cases to 123; the heatmap for these and the 12 normal control samples is shown in Fig. 1E. As described previously, hierarchical clustering identified three patient subgroups, two with coordinate expression of hypoxia and immune signature genes. Normal controls clustered with the hypoxia^low/immune^high subgroup, where p16-positive cases were also overrepresented. Conversely, the small hypoxia^high/immune^low subgroup was composed of a
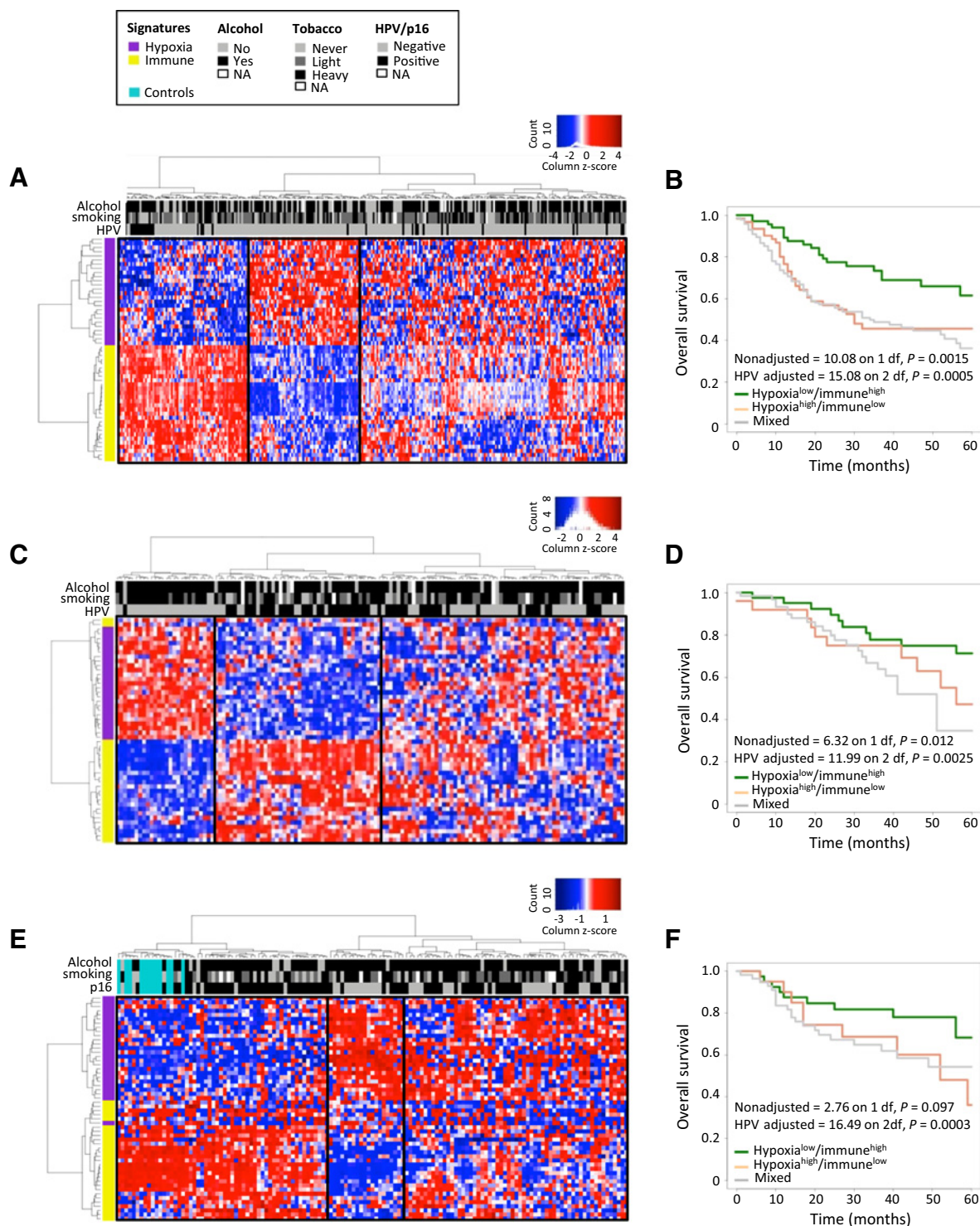
Figure 1.
Development and validation of hypoxia-immune prognostic classifier. Two-dimensional unsupervised hierarchical clustering identifies distinct HNC patient subgroups with coordinate expression of hypoxia- and immune response–related genes (red, high gene expression; white, intermediate gene expression; blue, low gene expression). Hypoxia (Eustace and colleagues) signature genes are colored purple and immune (CIRC) signature genes yellow, for TCGA (**A**), Chicago (**C**), and Correlate datasets (**E**). Alcohol consumption, tobacco use, and HPV/p16 status are represented per patient. Correlate dataset (**E**) includes 12 patients who underwent tonsillectomy for management of a nonmalignant process (snoring) colored cyan (controls). Kaplan–Meier survival plots for OS stratified according to the combined hypoxia-immune signature for TCGA ($n = 275$; **B**), Chicago ($n = 130$; **D**), and Correlate ($n = 123$; **F**) patient cohorts. Data are censored at 5 years. Log-rank P values are displayed for nonadjusted and HPV/p16 adjusted analyses.

majority of p16-negative cases. The mixed subgroup again included both HPV-positive and -negative cases, supporting the proposal that the hypoxia-immune signature classifies beyond HPV status (Fig. 1E). Despite the smaller subgroup size, Kaplan–Meier analysis revealed that the three subgroups have distinct outcome profiles, mirroring the TCGA results (Fig. 1F), with 5-year OS rates of 79.5%, 64.4%, and 55% for the hypoxia^{low}/immune^{high}, mixed and hypoxia^{high}/immune^{low} subgroups, respectively ($P = 0.097$; HPV-adjusted $P = 0.0003$).

Hypoxia may result from rapid tumor growth with inadequate neovascularization. To address the possibility that hypoxia-immune subgroup classification was significantly influenced by tumor volume the distribution of T stage within the three subgroups was examined. A correlation with T stage was not consistently observed (Supplementary Fig. S4).

Distribution of individual hypoxia- and immune-related gene expression within the three subgroups

The analyses described above identified three distinct HNC patient subgroups with coordinate expression of hypoxia- and immune-related gene signatures. However, within each group individual genes may differ in their expression and contribution to the endotype. Subsequent exploratory analyses therefore mapped expression of individual genes within the three subgroups in an attempt to understand their distinct contributions to each endotype. This analysis focused on the TCGA dataset where whole transcriptome data are available, enabling interrogation of genes of interest not included in the Chicago microarray or Correlate targeted sequencing datasets. As illustrated in Fig. 2 and Supplementary Fig. S5A, the pattern of expression for individual hypoxia-related genes was relatively broad with considerable overlap between subgroups, particularly the hypoxia^{high}/immune^{low} and mixed classes. However, a subset of genes showed greater differential expression (hypoxia^{high}/immune^{low} > mixed > hypoxia^{low}/immune^{high}) including *CA9*, *SLC2A1* (GLUT1), and *SLC16A1* (MCT1), the products of which are involved in pH regulation and glucose metabolism (Fig. 2, top; Supplementary Fig. S5A). Twenty-three of the 26 genes represented in the hypoxia signature showed significant differential expression between the hypoxia^{low}/immune^{high} and hypoxia^{high}/immune^{low} or mixed subgroups.

Immune response–related genes described by the CIRC signature were all differentially expressed, albeit to varying extents, according to the expected order: hypoxia^{low}/immune^{high} > mixed > hypoxia^{high}/immune^{low} (Fig. 2; Supplementary Fig. S5B). The majority of immune genes of interest outside of the CIRC signature also demonstrated a similar pattern of differential expression (Fig. 2; Supplementary Fig. S5C). This was true of genes whose products would be expected to mediate anti- or protumoral roles; for example, markers of cytotoxic and regulatory T-cell function. Genes associated with the myeloid lineage were also expressed at significantly higher levels within the hypoxia^{low}/immune^{high} subgroup; although markers of effector/suppressor function [e.g., *ARG1* and *NOS2* (iNOS)] were not uniformly coexpressed. Other genes of particular interest included those encoding activating receptors (e.g., CD40, CD137, and OX40) or inhibitory receptors (e.g., CTLA-4, LAG3, and PD-1) the ectonucleotidases CD39/CD73 and indoleamine 2,3-dioxygenase (IDO); as therapies targeting these markers are currently in clinical practice, trials, or in development. *IDO1* is one of six genes comprising an "IFNγ signature" that has shown predictive value for response to anti-

PD-1 mAb therapy in HNC and other cancers (19). The other five genes, all part of the CIRC signature, display a similar expression pattern: hypoxia^{low}/immune^{high} >> mixed > hypoxia^{high}/immune^{low}; these include *IFNG* itself and the chemokines *CXCL9*/*CXCL10*, which may be important for T-cell homing to tumors. Finally, *EGFR* was significantly overexpressed in the hypoxia^{high}/immune^{low} and mixed subgroups relative to the hypoxia^{low}/immune^{high} group.

Protein expression classifier

While gene signatures potentially better reflect the complex interactions between immune cells and the hypoxic tumor microenvironment, simplified IHC signatures may be more clinically applicable. Furthermore, gene expression may not correlate with end protein expression due to posttranscriptional or translational control and protein degradation. Finally, gene signatures neither discriminate between expression within tumor or stromal compartments, nor identify cell type–specific expression. Therefore, we next examined whether an IHC signature comprising TILs, CD3, PD-L1, and LAG3 as immune-response markers and CA-IX as a marker of hypoxia could stratify patients into the corresponding subgroups with different prognoses.

Results for individual markers are summarized in Supplementary Table S4; representative images showing the different patterns of expression and their association with OS are shown in Fig. 3 and Supplementary Fig. S6, with the corresponding statistical analyses in Supplementary Table S5. In agreement with previous studies, high TIL status (assessed on H & E staining) correlated with p16 status (3), and patients with the highest TIL numbers had a significantly better OS [HR 0.27; 95% confidence interval (CI), 0.12–0.66; $P = 0.004$ on univariate analysis]. Similarly, high numbers of T cells (measured by CD3 staining) correlated with improved OS [combined CD3: HR, 0.39; 95% CI, 0.2–0.77; $P = 0.007$ on univariate analysis). Because the precise location of T cells within the tumor microenvironment may impact on their prognostic significance (29), T-cell frequencies were independently evaluated for three locations: within tumor nests, within the peritumoral stroma, and at the tumor margin. An elevated frequency of intratumoral T cells showed the greatest prognostic value (HR, 0.33; 95% CI, 0.16–0.67; $P = 0.002$) and this was independent of clinical factors and p16 status [adjusted HR (aHR), 0.43; 95% CI, 0.19–0.97; $P = 0.043$; Fig. 3; Supplementary Table S5].

The prognostic impact of PD-L1 expression was dependent on both the cell types considered and the cutoff selected (Fig. 3C and H; Supplementary Fig. S6). Higher expression on tumor cells correlated with improved survival using one of the four tested cutoffs (25%; aHR, 0.33; 95% CI, 0.13–0.89; $P = 0.025$). Similarly, a trend for improved survival was observed for higher expression on intra-/peritumoral immune cells (HR, 0.45; 95% CI, 0.19–1.05; $P = 0.066$). In addition, the presence of a PD-L1–positive immune cordon around tumor nests was associated with better OS (aHR, 0.19; 95% CI, 0.05–0.68; $P = 0.011$). Using a CPS, which considers PD-L1 expression on both tumor and inflammatory cells, strengthened prediction of OS (Supplementary Table S5). Thus CPS based on ≥1%, ≥5%, and ≥25% cutoffs all predicted OS on multivariate analysis; only the ≥50% cutoff did not.

Results for the checkpoint receptor, LAG3, expressed on inflammatory cells showed a trend for improved survival with higher expression (Fig. 3D and I), particularly when these cells were
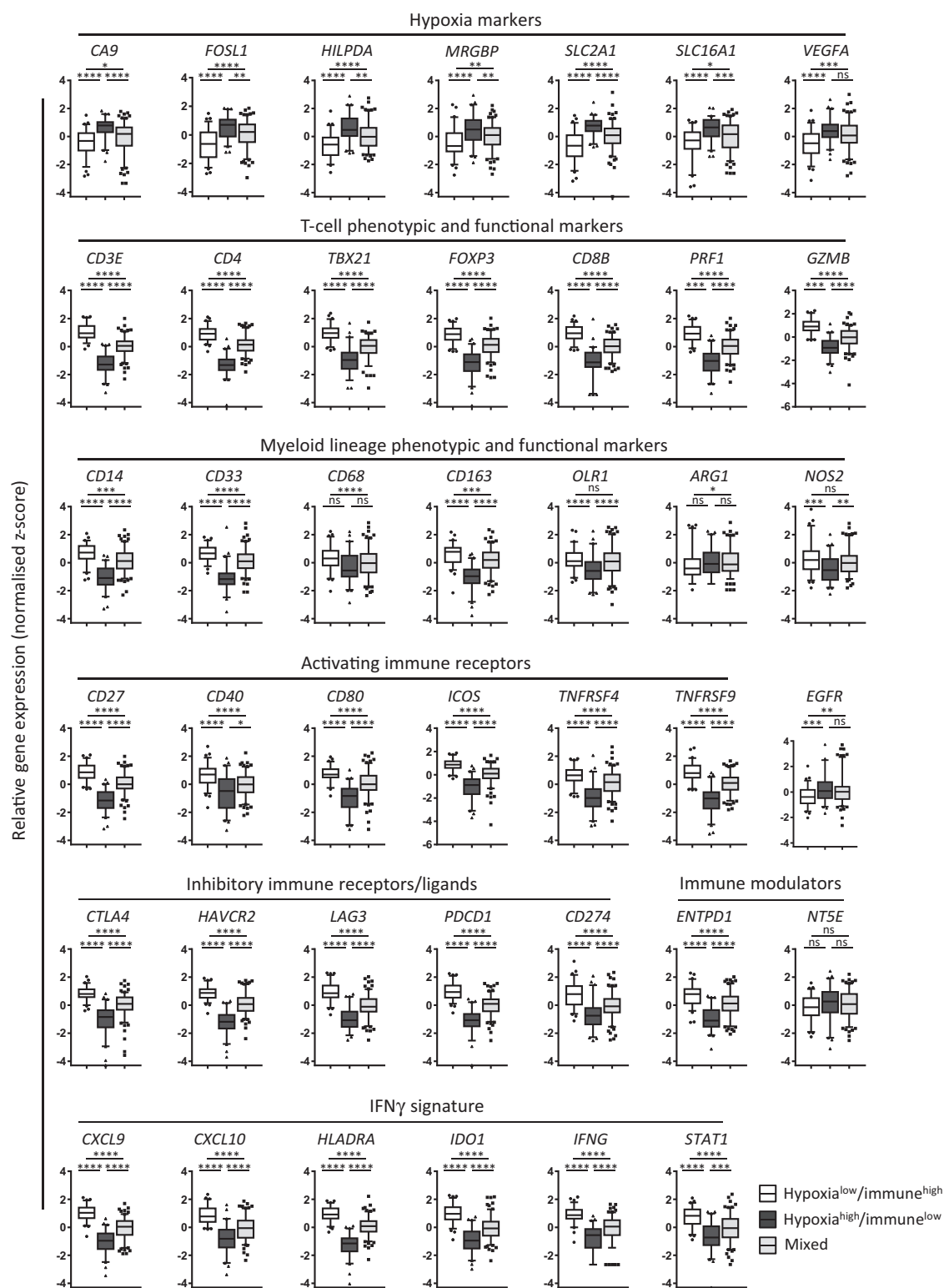
Figure 2.
Expression of individual hypoxia- or immune-response–related genes within the heatmap defined subgroups. Box and whisker plots showing normalized z-scores for selected genes of interest, acquired from TCGA dataset. The hypoxia[low]/immune[high], hypoxia[high]/immune[low], and mixed subgroups (as defined by two-dimensional unsupervised hierarchical clustering of gene expression) are represented as white, dark gray, and light gray, respectively. Data were analyzed using Kruskal–Wallis test with Dunn correction; P values are reported as: ns, nonsignificant; *, $P < 0.05$; **, $P < 0.005$; ***, $P < 0.0005$; ****, $P < 0.0001$.
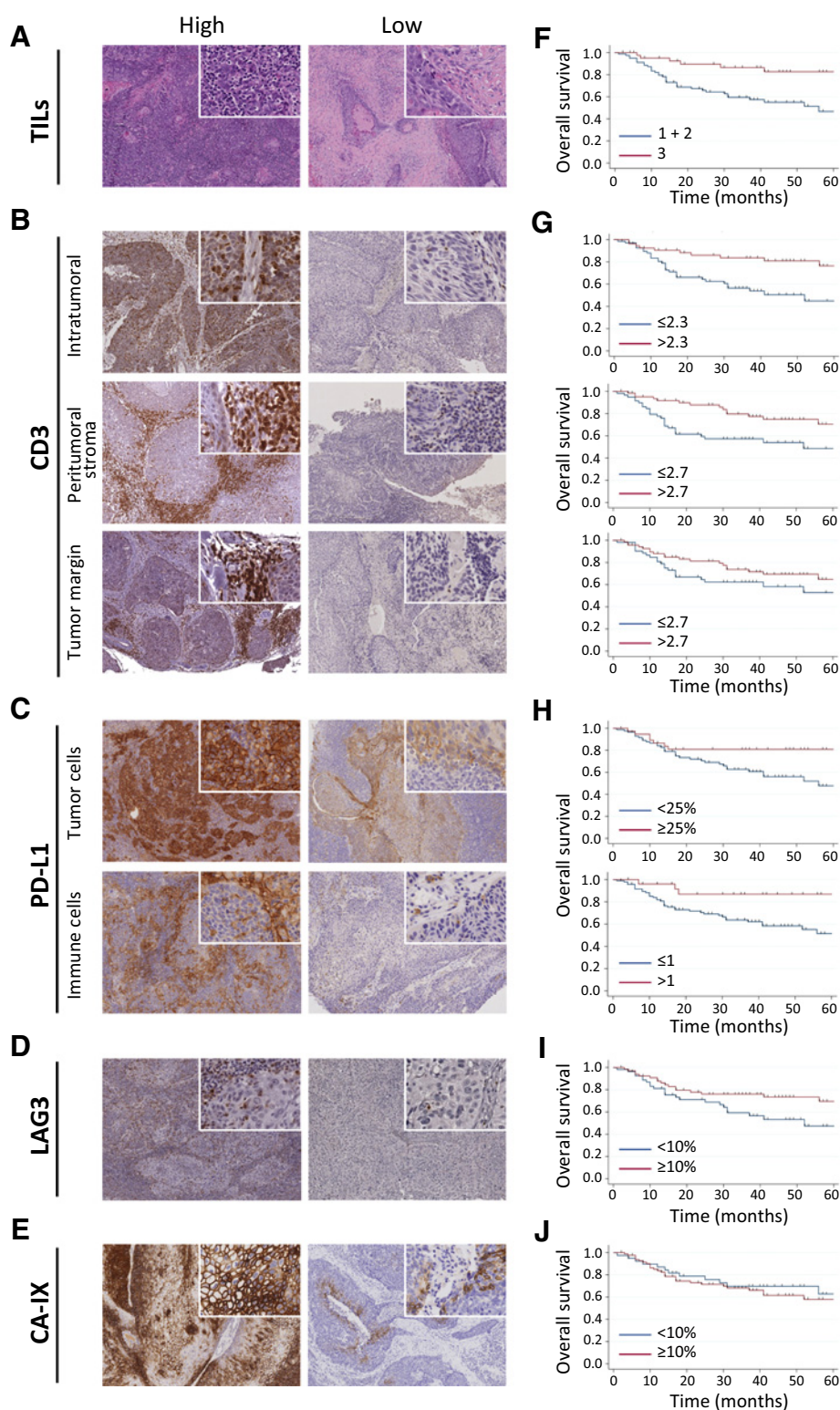
Figure 3.
IHC staining of selected immune- or hypoxia-marker expression and correlation with survival. Representative images showing high and low numbers of TILs (H & E; **A**); high and low expression of CD3 within different regions of the tumor (within tumor nests, the stroma proximal to the tumor and at the tumor periphery; **B**); constitutive versus inductive expression of PD-L1 on tumor cells (top) and distinct patterns of PD-L1 expression on immune cells within the tumor microenvironment (bottom; **C**). High and low expression of LAG3 on infiltrating immune cells (**D**); high and low CA-IX expression within tumor cells (**E**). Main images: original magnification 10×; inset: 40×. **F–J,** Kaplan–Meier curves for OS according to individual immune or hypoxia marker expression. Data were dichotomized into low (blue line) and high (red line) expression subgroups on the basis of the indicated cutoffs (for CD3 median value used) and censored at 5 years.

located within tumor nests (25% cutoff: HR, 0.34; 95% CI, 0.12–0.96; $P = 0.042$). However, these were not significant when adjusted for other tumor factors.

Two-thirds of tumors contained hypoxic regions as measured by CA-IX expression (≥10% cutoff). There are conflicting reports

in the literature regarding the prognostic value of CA-IX expression in HNC (reviewed in ref. 30). Here, CA-IX expression was not prognostic in the complete case analysis (Fig. 3J), although there was a trend for improved survival in the subset of patients with very low or absent expression when multiple imputation analysis

was used (HR 3.89, 95% CI, 0.95–16.00, $P = 0.060$; aHR 9.02, 95% CI, 1.96–41.59, $P = 0.005$; Supplementary Fig. S6).

Since both RNASeq and IHC data were available for the majority of samples from the Correlate cohort, we compared normalized gene versus protein expression levels and found a significant positive correlation for all examined hypoxia or immune markers (Supplementary Fig. S7). Subsequent analyses evaluated levels of IHC marker expression within the three heatmap gene cluster–defined subgroups (hypoxia[high]/immune[low], hypoxia[low]/immune[high], and mixed). All immune-related markers showed significantly higher levels of protein expression in the hypoxia[low]/immune[high] versus hypoxia[high]/immune[low] subgroups; expression levels for the mixed subgroup were intermediate. As expected, CA-IX protein expression was significantly decreased in the hypoxia[low]/immune[high] versus hypoxia[high]/immune[low] subgroups and intermediate in the mixed group (Fig. 4A).

Immune profile

It has been suggested that cancers, including HNC, can be assigned one of three immune profiles, based on the frequency and distribution of T cells within the tumor and microenvironment (25). Thus "immune deserts" are characterized by minimal T-cell presence, "immune-excluded" tumors are surrounded by abundant peritumoral T cells, but permit limited intratumoral penetration, and "inflamed tumors" contain relatively high numbers of T cells in both compartments—here T-cell function is apparently compromised. To explore a possible relationship between tumor immune profile and the three gene cluster–defined subgroups as above, all cases within the Correlate cohort were assigned an immune phenotype (desert/excluded/inflamed) based on the magnitude and pattern of CD3 staining. As illustrated in Fig. 4B, hypoxia[high]/immune[low] tumors were overrepresented in the "immune desert" category and significantly reduced in the inflamed subgroup. The reverse pattern was observed for hypoxia[low]/immune[high] tumors; while tumors classified as mixed on the basis of hypoxia-immune gene expression were more evenly distributed across all three immune profiles.

Spatial interactions of immune cells and hypoxia in the tumor microenvironment

In the final series of experiments, we examined the spatial distribution of different cell populations within the tumor microenvironment, in particular the relationship between regions of tumor hypoxia (as measured by CA-IX expression), immune cell localization and PD-L1 expression. Fifteen cases, representative of the three hypoxia-immune subgroups identified in the gene expression analyses, were stained using Opal Multiplex IHC assays. Representative images are shown in Fig. 5 and Supplementary Fig. S8. Staining for cytokeratin (as a marker for tumor cells) confirmed that CA-IX expression is restricted to tumor cells (Supplementary Fig. S8A). A subset of tumors with high levels of CA-IX expression displayed an "immune desert" phenotype, with few T cells present in either the stromal or tumoral compartments (Fig. 5A; hypoxia[high]/immune[low]). In other cases, abundant T cells were observed within the peritumoral stroma, but minimal numbers appeared to have infiltrated tumor nests, consistent with an "immune excluded" phenotype (Fig. 5B; mixed; Supplementary Fig. S8B and S8C). The final category comprised "inflamed" tumors with abundant T cells present in the peritumoral stroma

and significant intratumoral infiltration, particularly in the absence of hypoxia as indicated by no/minimal CA-IX expression (Fig. 5C, hypoxia^{low}/immune^{high}). Overall, we observed a significant inverse correlation between CA-IX positivity and the prevalence of CD3^{+} T cells within tumor nests (Fig. 5D, left; $r = -0.5464$; $P = 0.0377$,) but not within the stromal compartment alone (Fig. 5D, middle; $r = -0.2393$; $P = 0.3982$) or the combined tumor environment (Fig. 5D, right; $r = -0.4571$; $P = 0.0889$), consistent with hypoxia-mediated inhibition of T-cell migration and/or survival within tumor nests. No significant correlation was observed between tumoral expression of CA-IX and PD-L1 (Supplementary Fig. S8D), which is unsurprising given that hypoxia (via HIF1α) is only one of multiple potential pathways leading to PD-L1 expression. Excepting "constitutive" cases, strong tumoral PD-L1 expression was restricted to cells at the stromal interface, found in close proximity to CD3-positive T cells (Fig. 5B and C, yellow triangles). The positive correlation between stromal PD-L1 and CD3 T cells (Fig. 5E) is consistent with a dominant role for IFNγ-mediated expression.

Discussion

Recent studies have advanced our understanding of the biological and molecular characteristics of HNC (4–7). However, there remains an unmet need for clinically relevant classifications to guide therapy selection. Key features associated with the biologically distinct subtypes include immune landscape, expression of EGFR/HER, and hypoxia (7, 31). Given the strong evidential basis for efficacy of hypoxia modification (reviewed in ref. 18) and immune checkpoint inhibitors (19, 20) in the treatment of HNC, we explored a combination of hypoxia and immune status classifiers. Use of the hypoxia-immune signature in an unsupervised cross-cohort manner identified three distinct HNC subtypes. Subgroup classification correlated with survival, with the hypoxia[low]/immune[high] subgroup having the best prognosis. The hypoxia[high]/immune[low] and mixed subgroups have similar survival profiles; however, they have distinct transcriptional patterns and immune profiles, consistent with activated pathways that could be targeted by different therapeutic interventions, hence the importance of separating them.

Given the widespread use of IHC for diagnostic purposes in routine pathology practice, we evaluated whether a simplified IHC-based signature could substitute for the developed hypoxia-immune gene expression signature. Expression of individual immune response markers, notably intratumoral CD3^{+} T cells and PD-L1 expression (assessed using a CPS) correlated with superior outcome, but did not improve the prognostic value of clinical factors alone. CA-IX, as a marker of hypoxia, did not have prognostic power.

Finally, consistent with hypoxia-driven immune suppression, multiplex IHC staining identified an inverse relationship between CA-IX and infiltration of CD3 T cells into tumor regions. The observed spatial distribution of hypoxia and immune response markers within the tumor microenvironment correlated strongly with our classification based on gene expression, confirming its validity.

An inverse correlation between hypoxia-related gene expression and antitumoral immune responses is consistent with previous studies in HNC (7, 31). As mentioned above, hypoxia drives immune suppression via multiple mechanisms. It may be achieved through HIF1α-mediated activation of inhibitory
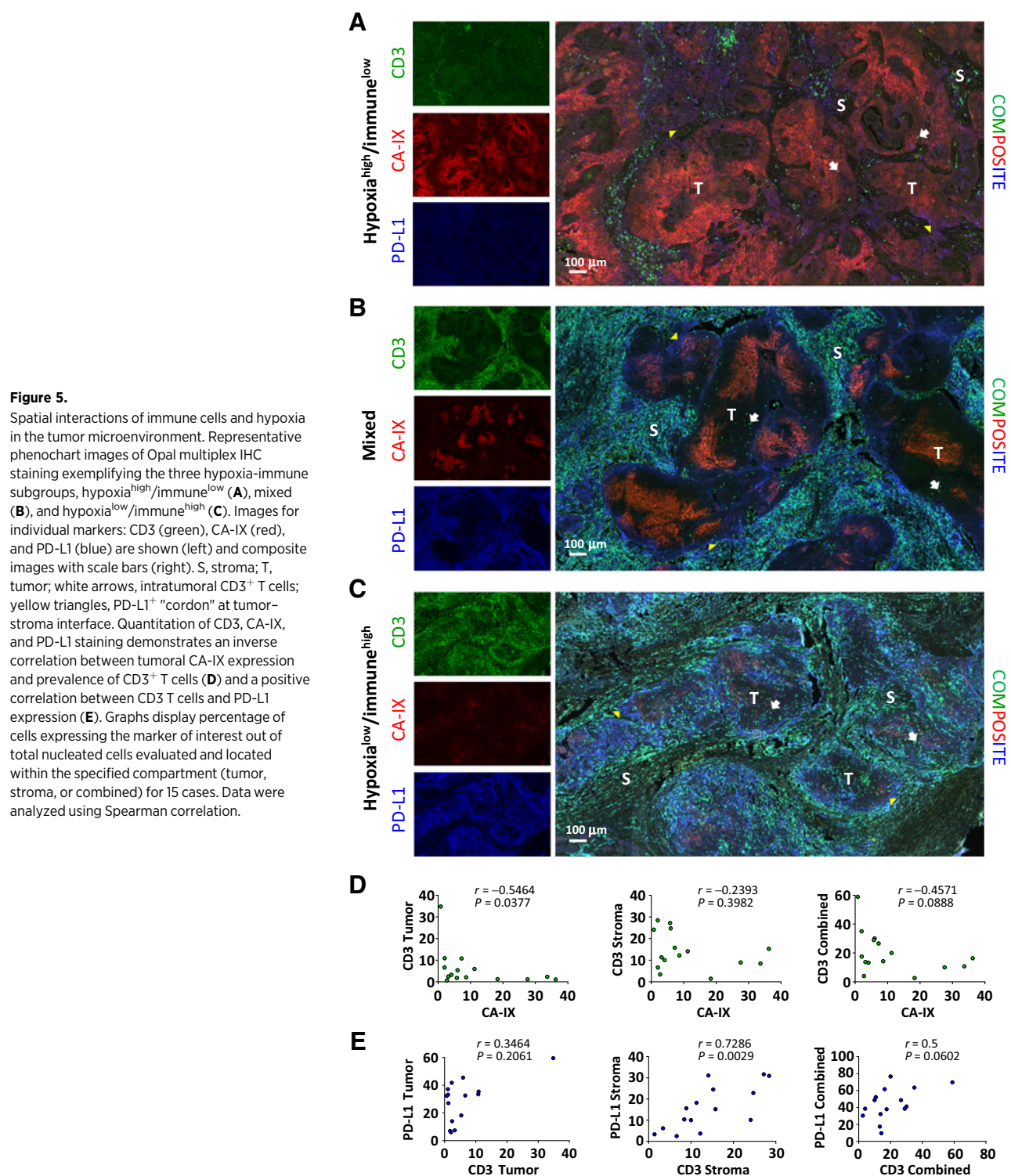
Brooks et al.
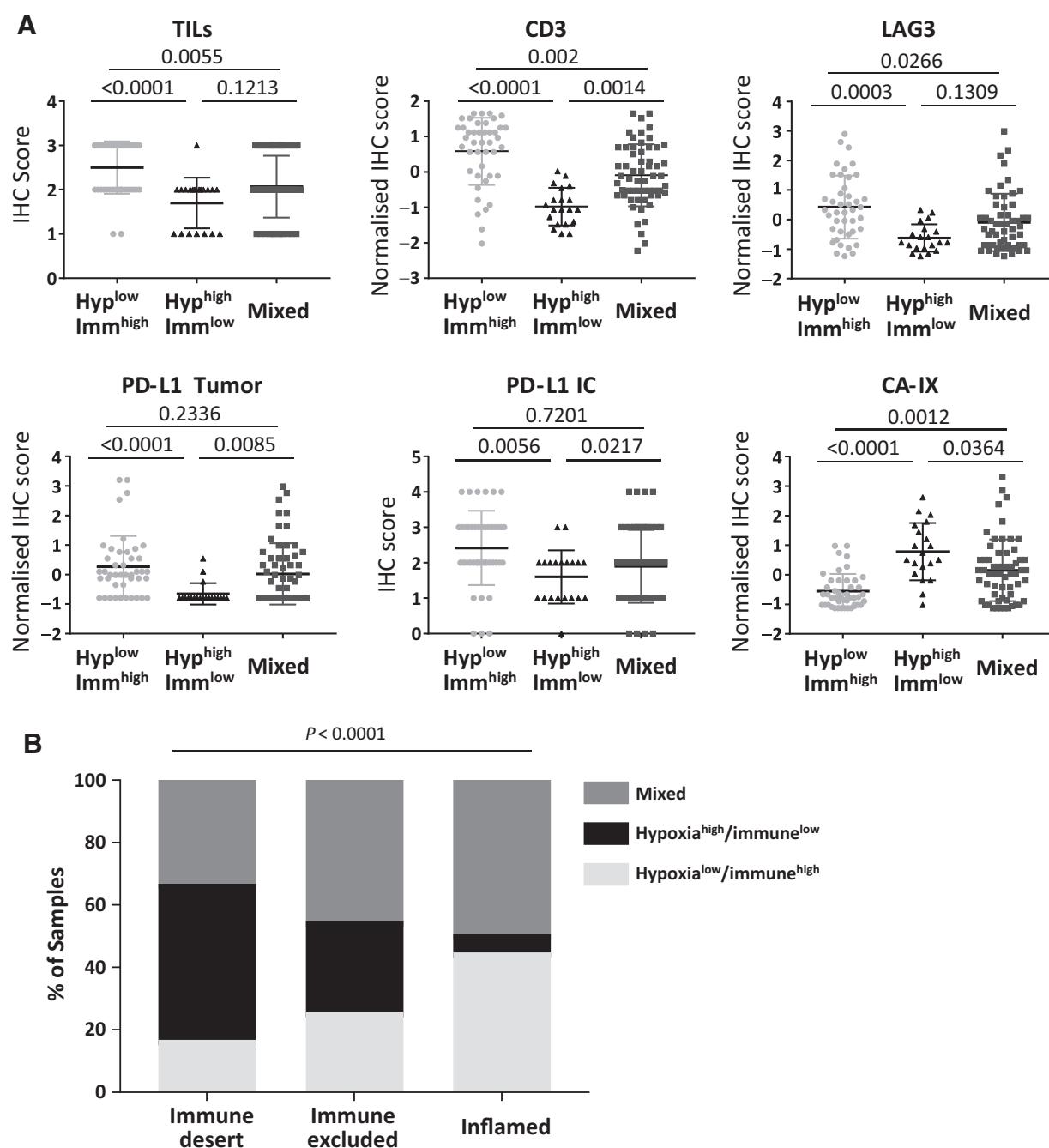
Figure 4.
Relationship between heatmap groups, IHC marker expression, and immune profile. **A,** All cases where both protein and gene expression data were available ($n = 123$) were subdivided into the three gene cluster–defined subgroups and IHC marker expression scatterplots generated using raw scores (TILs and PD-L1 on immune cells) or z-scores (CD3, PD-L1 tumor, LAG3, and CA-IX). Bars, mean with SD. Data were analyzed using Kruskal–Wallis test with Dunn correction; exact P values are reported. **B,** The 123 cases were assigned an immune profile (desert, excluded, or inflamed) based on their CD3 IHC score. Graph shows percentage of samples within each immune phenotype belonging to the three heatmap gene cluster–defined subgroups. Data were analyzed using Fisher exact test.

pathways, including CD47 (32), the adenosine-generating enzymes CD73 and CD39 (33), and immune checkpoint receptors such as PD-L1 (11, 12). Perhaps paradoxically, many inhibitory markers are more highly expressed in "inflamed" tumors (hypoxia^{low}/immune^{high}), where they may be indicative of an ongoing "exhausted" antitumor immune response (34), with the potential for reactivation via immune checkpoint blockade. Tumor cell metabolic adaptations to hypoxia, such as increased glucose uptake and lactate production, also act to promote and perpetuate an immunosuppressive

Figure 5.
Spatial interactions of immune cells and hypoxia in the tumor microenvironment. Representative phenochart images of Opal multiplex IHC staining exemplifying the three hypoxia-immune subgroups, hypoxia^{high}/immune^{low} (**A**), mixed (**B**), and hypoxia^{low}/immune^{high} (**C**). Images for individual markers: CD3 (green), CA-IX (red), and PD-L1 (blue) are shown (left) and composite images with scale bars (right). S, stroma; T, tumor; white arrows, intratumoral CD3$^+$ T cells; yellow triangles, PD-L1$^+$ "cordon" at tumor–stroma interface. Quantitation of CD3, CA-IX, and PD-L1 staining demonstrates an inverse correlation between tumoral CA-IX expression and prevalence of CD3$^+$ T cells (**D**) and a positive correlation between CD3 T cells and PD-L1 expression (**E**). Graphs display percentage of cells expressing the marker of interest out of total nucleated cells evaluated and located within the specified compartment (tumor, stroma, or combined) for 15 cases. Data were analyzed using Spearman correlation.

microenvironment (9, 10). Because of differences in their metabolic programs these factors would be expected to have greater impact on effector versus regulatory T cells (35). Alternatively, because most hypoxic tumor areas contained minimal T cells (immune desert or excluded profile), immune suppression may be mediated mainly by mechanisms that inhibit T-cell migration into tumors (e.g., VEGF and CXCL12) or promote T-cell death (e.g., FasL; reviewed in 36).

As described here and reported previously (31), "inflamed" (hypoxia^{low}/immune^{high}) tumors demonstrate robust myeloid gene expression profiles. The balance of antitumoral versus immunosuppressive function of myeloid cells, including

myeloid-derived suppressor cells (MDSCs) and tumor-associated macrophages (TAMs), may be modulated by tumor hypoxia, which favors suppression (8, 11, 13). Mechanistically, hypoxia (predominantly via HIF signaling) can tip the balance of cytokine/chemokine/effector molecule production toward those with protumoral functions (e.g., IL10, VEGF, arginase, and iNOS) and also upregulate expression of T-cell inhibitory ligands (e.g., PD-L1).

Hypoxia can upregulate EGFR expression (37, 38) and promote ligand-independent EGFR signaling (39), both mechanisms potentially augmenting tumor glycolytic metabolism and consequent metabolic competition. EGFR overexpression is observed in a high percentage of HNC, particularly HPV-negatives cases, and is associated with poor prognosis; other mechanisms of upregulation include mutations, gene duplications, and protein stabilization (reviewed in ref. 40). As previously mentioned, EGFR signaling may lead to hypoxia-independent stabilization of HIF1α and consequent upregulation of glycolytic metabolism (15, 16); providing an alternative (not mutually exclusive) explanation for low intratumoral T-cell infiltration (31). However, it is noteworthy that hypoxic modification appears most beneficial for patients with HPV-negative tumors (41, 42), consistent with an important role for hypoxia-mediated HIF1α upregulation. Furthermore, it has been reported that oropharyngeal tumors, especially HPV-positive tumors are less hypoxic (43).

T-cell infiltration of tumors (especially by CD8$^+$ cytotoxic T lymphocytes) has been associated with a favorable prognosis in several tumor types, including HNC (3, 24, 29, 44). Likewise, PD-L1 expression, particularly within immune cells in the tumor microenvironment, can have both prognostic and predictive importance (26, 27). In our study, higher numbers of TILs and CD3$^+$ T cells, particularly within tumor nests, correlated with improved survival. PD-L1 expression was also linked with better prognosis (dependent on cutoff), especially when both tumor and immune cell expression were considered as a CPS. The differential prognostic impact of intermediate (CPS > 1% and <50%) versus high ($\geq$50%) PD-L1 expression might reflect alternative mechanisms controlling expression. Intermediate expression (found on immune cells and tumor cells at the stromal interface) may be indicative of adaptive immune resistance in the face of an ongoing antitumoral immune response (45, 46); whereas high levels are associated with tumor intrinsic expression (e.g., loss of PTEN or EGFR activation; refs. 47, 48).

Previous studies in diverse tumor settings have correlated response to immune checkpoint blockade (particularly involving the PD-1/PD-L1 axis) with "cancer immune phenotype" (25). Thus "inflamed" tumors exhibit higher response rates compared with those having "immune desert" or "immune excluded" profiles, although even in the former cases a response is not assured. Our combined analysis of gene and protein expression in HNC suggests that hypoxia may be an important factor distinguishing hot (inflamed) and cold (immune desert or excluded) tumors. In agreement with this, it has recently been reported that targeted hypoxia reduction restores intratumoral T-cell infiltration in a mouse model of prostate cancer (49).

We recognize certain limitations in our study, including the potential for bias due to different tumor:stroma ratios within samples; for example, TCGA samples comprise >80% tumor cells, therefore reducing analysis of the stromal compartment. Minor intercohort variations in gene clustering and prognostic value of the classifier (as measured by 5-year OS) may reflect (i)

different RNA quantification platforms (microarray vs. whole-transcriptome sequencing vs. targeted sequencing), (ii) fresh-frozen versus FFPE tissue, and (iii) differences in case mix (anatomic site, TNM/clinical stage, smoking, alcohol consumption, and HPV status) or treatment. Of note, the consistent performance of the classifier despite the heterogeneous nature of the study cohorts and assays is an indication of the strength of the signature (50). Currently, subgroup classification is based on gene clustering (three highest order clusters) rather than defined cutoffs. For clinical application, future work will need to define appropriate cutoffs, for example using median values (22) and/or develop a clinically applicable continuous scoring system.

The identification of our hypoxia-immune prognostic classifier for HNC suggests that differential treatment approaches might be required for patient subgroups. Although hypoxic modification (nimorazole) and immune checkpoint therapies (PD-1/PD-L1 inhibitors) have shown single-agent activity in HNC, the response rate is relatively low; for example, only 13%–18% for PD-1 in the recurrent/metastatic setting (19, 20). Our data suggest that combinations or sequential use of hypoxia-modifying and/or immunomodulatory drugs may be beneficial. For example, in patients with a hypoxia^{high}/immune^{low} or mixed signature correlating with poor prognosis, treatment with hypoxia modifiers may sensitize to chemo/radiotherapy, and EGFR inhibitors or agents targeting MDSCs/TAMs may reverse the immunosuppressive environment. Sequential treatment with immune checkpoint inhibitors may then be required to prevent inhibition or dampening of the emerging immune response. Cases that are hypoxia^{high}/immune^{high} might benefit from concurrent treatment with hypoxia modifiers and immune oncology agents. Importantly, our data on expression of individual genes also indicate potential for immunotherapy treatment strategies beyond PD-L1, for example combinations of PD-L1 and anti-LAG3 treatments for the hypoxia^{low}/immune^{high} subgroup.

In conclusion, we developed and validated a prognostic molecular classifier based on hypoxia and immune status. This classifier may have clinical application to guide the use of hypoxia modification and targeted immunotherapies such as checkpoint inhibitors. We would recommend validation of its prognostic value and assessment of any potential predictive power (e.g., using treatment with nimorazole, EGFR inhibitors, or anti-PD-1/PD-L1) in a prospective setting.

Disclosure of Potential Conflicts of Interest

Authors' Contributions

Conception and design: J.M. Brooks, N. Lal, R.J. Spruce, N. Batis, S.P. Lee, G. Middleton, D.A. Tennant, B.E. Willcox, H. Mehanna
Development of methodology: J.M. Brooks, A.N. Menezes, N. Lal, C.J. Bagnall, S.V. von Zeidler, D.A. Tennant, A.D. Beggs, J.-B. Cazier, B.E. Willcox, H. Mehanna

References

1. Ferlay J, Soerjomataram I, Dikshit R, Eser S, Mathers C, Rebelo M, et al. Cancer incidence and mortality worldwide: sources, methods and major patterns in GLOBOCAN 2012. Int J Cancer 2015;136:E359–86.
2. Ang KK, Harris J, Wheeler R, Weber R, Rosenthal DI, Nguyen-Tan PF, et al. Human papillomavirus and survival of patients with oropharyngeal cancer. N Engl J Med 2010;363:24–35.
3. Ward MJ, Thirdborough SM, Mellows T, Riley C, Harris S, Suchak K, et al. Tumour-infiltrating lymphocytes predict for outcome in HPV-positive oropharyngeal cancer. Br J Cancer 2014;110:489–500.
4. Chung CH, Parker JS, Karaca G, Wu J, Funkhouser WK, Moore D, et al. Molecular classification of head and neck squamous cell carcinomas using patterns of gene expression. Cancer Cell 2004;5:489–500.
5. Walter V, Yin X, Wilkerson MD, Cabanski CR, Zhao N, Du Y, et al. Molecular subtypes in head and neck cancer exhibit distinct patterns of chromosomal gain and loss of canonical cancer genes. PLoS One 2013;8:e56823.
6. Cancer Genome Atlas Network. Comprehensive genomic characterization of head and neck squamous cell carcinomas. Nature 2015;517:576–82.
7. Keck MK, Zuo Z, Khattri A, Stricker TP, Brown CD, Imanguli M, et al. Integrative analysis of head and neck cancer identifies two biologically distinct HPV and three non-HPV subtypes. Clin Cancer Res 2015;21:870–81.
8. Chouaib S, Noman MZ, Kosmatopoulos K, Curran MA. Hypoxic stress: obstacles and opportunities for innovative immunotherapy of cancer. Oncogene 2017;36:439–45.
9. Ho PC, Bihuniak JD, Macintyre AN, Staron M, Liu X, Amezquita R, et al. Phosphoenolpyruvate is a metabolic checkpoint of anti-tumor T cell responses. Cell 2015;162:1217–28.
10. Chang CH, Qiu J, O'Sullivan D, Buck MD, Noguchi T, Curtis JD, et al. Metabolic competition in the tumor microenvironment is a driver of cancer progression. Cell 2015;162:1229–41.
11. Noman MZ, Desantis G, Janji B, Hasmim M, Karray S, Dessen P, et al. PD-L1 is a novel direct target of HIF-1alpha, and its blockade under hypoxia enhanced MDSC-mediated T cell activation. J Exp Med 2014;211:781–90.
12. Barsoum IB, Smallwood CA, Siemens DR, Graham CH. A mechanism of hypoxia-mediated escape from adaptive immunity in cancer cells. Cancer Res 2014;74:665–74.
13. Corzo CA, Condamine T, Lu L, Cotter MJ, Youn JI, Cheng P, et al. HIF-1alpha regulates function and differentiation of myeloid-derived suppressor cells in the tumor microenvironment. J Exp Med 2010;207:2439–53.
14. Facciabene A, Peng X, Hagemann IS, Balint K, Barchetti A, Wang LP, et al. Tumour hypoxia promotes tolerance and angiogenesis via CCL28 and T (reg) cells. Nature 2011;475:226–30.
15. Phillips RJ, Mestas J, Gharaee-Kermani M, Burdick MD, Sica A, Belperio JA, et al. Epidermal growth factor and hypoxia-induced expression of CXC chemokine receptor 4 on non-small cell lung cancer cells is regulated by the phosphatidylinositol 3-kinase/PTEN/AKT/mammalian target of rapamycin signaling pathway and activation of hypoxia inducible factor-1alpha. J Biol Chem 2005;280:22473–81.
16. Peng XH, Karna P, Cao Z, Jiang BH, Zhou M, Yang L. Cross-talk between epidermal growth factor receptor and hypoxia-inducible factor-1alpha signal pathways increases resistance to apoptosis by up-regulating survivin gene expression. J Biol Chem 2006;281:25903–14.
17. Overgaard J, Hansen HS, Overgaard M, Bastholt L, Berthelsen A, Specht L, et al. A randomized double-blind phase III study of nimorazole as a hypoxic radiosensitizer of primary radiotherapy in supraglottic larynx and pharynx carcinoma. Results of the Danish Head and Neck Cancer Study (DAHANCA) Protocol 5-85. Radiother Oncol 1998;46:135–46.
18. Overgaard J. Hypoxic modification of radiotherapy in squamous cell carcinoma of the head and neck–a systematic review and meta-analysis. Radiother Oncol 2011;100:22–32.
19. Seiwert TY, Burtness B, Mehra R, Weiss J, Berger R, Eder JP, et al. Safety and clinical activity of pembrolizumab for treatment of recurrent or metastatic squamous cell carcinoma of the head and neck (KEYNOTE-012): an open-label, multicentre, phase 1b trial. Lancet Oncol 2016;17:956–65.
20. Ferris RL, Blumenschein G, Fayette J, Guigay J, Colevas AD, Licitra L, et al. Nivolumab for recurrent squamous-cell carcinoma of the head and neck. N Engl J Med 2016;375:1856–67.
21. Jordan RC, Lingen MW, Perez-Ordonez B, He X, Pickard R, Koluder M, et al. Validation of methods for oropharyngeal cancer HPV status determination in US cooperative group trials. Am J Surg Pathol 2012;36:945–54.
22. Eustace A, Mani N, Span PN, Irlam JJ, Taylor J, Betts GN, et al. A 26-gene hypoxia signature predicts benefit from hypoxia-modifying therapy in laryngeal cancer but not bladder cancer. Clin Cancer Res 2013;19:4879–88.
23. Lal N, Beggs AD, Willcox BE, Middleton GW. An immunogenomic stratification of colorectal cancer: Implications for development of targeted immunotherapy. Oncoimmunology 2015;4:e976052.
24. Dahlin AM, Henriksson ML, Van Guelpen B, Stenling R, Oberg A, Rutegard J, et al. Colorectal cancer prognosis depends on T-cell infiltration and molecular characteristics of the tumor. Mod Pathol 2011;24:671–82.
25. Chen DS, Mellman I. Elements of cancer immunity and the cancer-immune set point. Nature 2017;541:321–30.
26. Herbst RS, Soria JC, Kowanetz M, Fine GD, Hamid O, Gordon MS, et al. Predictive correlates of response to the anti-PD-L1 antibody MPDL3280A in cancer patients. Nature 2014;515:563–7.
27. Kim HR, Ha SJ, Hong MH, Heo SJ, Koh YW, Choi EC, et al. PD-L1 expression on immune cells, but not on tumor cells, is a favorable prognostic factor for head and neck cancer patients. Sci Rep 2016;6:36956.
28. De Meulenaere A, Vermassen T, Aspeslagh S, Huvenne W, Van Dorpe J, Ferdinande L, et al. Turning the tide: clinical utility of PD-L1 expression in squamous cell carcinoma of the head and neck. Oral Oncol 2017;70:34–42.

Brooks et al.

29. Galon J, Costes A, Sanchez-Cabo F, Kirilovsky A, Mlecnik B, Lagorce-Pages C, et al. Type, density, and location of immune cells within human colorectal tumors predict clinical outcome. Science 2006;313: 1960–4.

30. Swartz JE, Pothen AJ, Stegeman I, Willems SM, Grolman W. Clinical implications of hypoxia biomarker expression in head and neck squamous cell carcinoma: a systematic review. Cancer Med 2015;4:1101–16.

31. Ottensmeier CH, Perry KL, Harden EL, Stasakova J, Jenei V, Fleming J, et al. Upregulated glucose metabolism correlates inversely with CD8+ T-cell Infiltration and survival in squamous cell carcinoma. Cancer Res 2016;76: 4136–48.

32. Zhang H, Lu H, Xiang L, Bullen JW, Zhang C, Samanta D, et al. HIF-1 regulates CD47 expression in breast cancer cells to promote evasion of phagocytosis and maintenance of cancer stem cells. Proc Natl Acad Sci U S A 2015;112:E6215–23.

33. Allard B, Longhi MS, Robson SC, Stagg J. The ectonucleotidases CD39 and CD73: novel checkpoint inhibitor targets. Immunol Rev 2017;276: 121–44.

34. Pauken KE, Wherry EJ. Overcoming T cell exhaustion in infection and cancer. Trends Immunol 2015;36:265–76.

35. Siska PJ, Rathmell JC. T cell metabolic fitness in antitumor immunity. Trends Immunol 2015;36:257–64.

36. Joyce JA, Fearon DT. T cell exclusion, immune privilege, and the tumor microenvironment. Science 2015;348:74–80.

37. Franovic A, Gunaratnam L, Smith K, Robert I, Patten D, Lee S. Translational up-regulation of the EGFR by tumor hypoxia provides a nonmutational explanation for its overexpression in human cancer. Proc Natl Acad Sci U S A 2007;104:13092–7.

38. Misra A, Pandey C, Sze SK, Thanabalu T. Hypoxia activated EGFR signaling induces epithelial to mesenchymal transition (EMT). PLoS One 2012;7: e49766.

39. Wang Y, Roche O, Xu C, Moriyama EH, Heir P, Chung J, et al. Hypoxia promotes ligand-independent EGF receptor signaling via hypoxia-inducible factor-mediated upregulation of caveolin-1. Proc Natl Acad Sci U S A 2012;109:4892–7.

40. Mirghani H, Amen F, Moreau F, Guigay J, Hartl DM, Lacau St Guily J. Oropharyngeal cancers: relationship between epidermal growth factor receptor alterations and human papillomavirus status. Eur J Cancer 2014;50:1100–11.

41. Lassen P, Eriksen JG, Hamilton-Dutoit S, Tramm T, Alsner J, Overgaard J, et al. HPV-associated p16-expression and response to hypoxic modification of radiotherapy in head and neck cancer. Radiother Oncol 2010;94: 30–5.

42. Rischin D, Young RJ, Fisher R, Fox SB, Le QT, Peters LJ, et al. Prognostic significance of p16INK4A and human papillomavirus in patients with oropharyngeal cancer treated on TROG 02.02 phase III trial. J Clin Oncol 2010;28:4142–8.

43. Tawk B, Schwager C, Deffaa O, Dyckhoff G, Warta R, Linge A, et al. Comparative analysis of transcriptomics based hypoxia signatures in head-and neck squamous cell carcinoma. Radiother Oncol 2016;118:350–8.

44. Balermpas P, Michel Y, Wagenblast J, Seitz O, Weiss C, Rodel F, et al. Tumour-infiltrating lymphocytes predict response to definitive chemoradiotherapy in head and neck cancer. Br J Cancer 2014;110:501–9.

45. Tumeh PC, Harview CL, Yearley JH, Shintaku IP, Taylor EJ, Robert L, et al. PD-1 blockade induces responses by inhibiting adaptive immune resistance. Nature 2014;515:568–71.

46. Lyford-Pike S, Peng SW, Young GD, Taube JM, Westra WH, Akpeng B, et al. Evidence for a role of the PD-1:PD-L1 pathway in immune resistance of HPV-associated head and neck squamous cell carcinoma. Cancer Research 2013;73:1733–41.

47. Parsa AT, Waldron JS, Panner A, Crane CA, Parney IF, Barry JJ, et al. Loss of tumor suppressor PTEN function increases B7-H1 expression and immunoresistance in glioma. Nat Med 2007;13:84–8.

48. Concha-Benavente F, Srivastava RM, Trivedi S, Lei Y, Chandran U, Seethala RR, et al. Identification of the cell-intrinsic and -extrinsic pathways downstream of EGFR and IFNgamma that induce PD-L1 expression in head and neck cancer. Cancer Res 2016;76:1031–43.

49. Jayaprakash P, Ai M, Liu A, Budhani P, Bartkowiak T, Sheng J, et al. Targeted hypoxia reduction restores T cell infiltration and sensitizes prostate cancer to immunotherapy. J Clin Invest 2018;128:5137–49.

50. Moons KG, Altman DG, Reitsma JB, Ioannidis JP, Macaskill P, Steyerberg EW, et al. Transparent reporting of a multivariable prediction model for Individual Prognosis or Diagnosis (TRIPOD): explanation and elaboration. Ann Intern Med 2015;162:W1–73.

Clinical Cancer Research

Development and Validation of a Combined Hypoxia and Immune Prognostic Classifier for Head and Neck Cancer

Jill M. Brooks, Albert N. Menezes, Maha Ibrahim, et al.

Updated version	Access the most recent version of this article at: doi:10.1158/1078-0432.CCR-18-3314
Supplementary Material	Access the most recent supplemental material at: http://clincancerres.aacrjournals.org/content/suppl/2019/06/08/1078-0432.CCR-18-3314.DC1

Cited articles	This article cites 50 articles, 16 of which you can access for free at: http://clincancerres.aacrjournals.org/content/25/17/5315.full#ref-list-1
Citing articles	This article has been cited by 1 HighWire-hosted articles. Access the articles at: http://clincancerres.aacrjournals.org/content/25/17/5315.full#related-urls

E-mail alerts	Sign up to receive free email-alerts related to this article or journal.
Reprints and Subscriptions	To order reprints of this article or to subscribe to the journal, contact the AACR Publications Department at pubs@aacr.org.
Permissions	To request permission to re-use all or part of this article, use this link http://clincancerres.aacrjournals.org/content/25/17/5315. Click on "Request Permissions" which will take you to the Copyright Clearance Center's (CCC) Rightslink site.